THE JOURNAL OF BIOLOGICAL CHEMISTRY VOL. 286, NO. 30, pp. 26496–26506, July 29, 2011
Printed in the U.S.A.

A Kinase Anchor Protein 150 (AKAP150)-associated Protein Kinase A Limits Dendritic Spine Density*

Received for publication, April 26, 2011, and in revised form, June 2, 2011 Published, JBC Papers in Press, June 7, 2011, DOI 10.1074/jbc.M111.254912

Yuan Lu[‡§1], Xiang-ming Zha[¶‖], Eun Young Kim[**], Scott Schachtele[¶], Michael E. Dailey[¶], Duane D. Hall[‡], Stefan Strack[‡], Steven H. Green[¶], Dax A. Hoffman[**], and Johannes W. Hell[‡ ‡‡2]

*From the [‡]Department of Pharmacology, Roy J. and Lucille A. Carver College of Medicine and the [¶]Department of Biology, College of Liberal Arts and Sciences, University of Iowa, Iowa City, Iowa 52242, the [§]Genes, Cognition and Psychosis Program, National Institute of Mental Health, Bethesda, Maryland 20892, the [‖]Department of Cell Biology and Neuroscience, College of Medicine, University of South Alabama, Mobile, Alabama 36688, the **Molecular Neurophysiology and Biophysics Unit, Eunice Kennedy Shriver National Institute of Child Health and Human Development, National Institutes of Health, Bethesda, Maryland 20892, and the [‡‡]Department of Pharmacology, School of Medicine, University of California, Davis, California 95615*

The A kinase anchor protein AKAP150 recruits the cAMP-dependent protein kinase (PKA) to dendritic spines. Here we show that in AKAP150 (AKAP5) knock-out (KO) mice frequency of miniature excitatory post-synaptic currents (mEPSC) and inhibitory post-synaptic currents (mIPSC) are elevated at 2 weeks and, more modestly, 4 weeks of age in the hippocampal CA1 area *versus* litter mate WT mice. Linear spine density and ratio of AMPAR to NMDAR EPSC amplitudes were also increased. Amplitude and decay time of mEPSCs, decay time of mIPSCs, and spine size were unaltered. Mice in which the PKA anchoring C-terminal 36 residues of AKAP150 are deleted (D36) showed similar changes. Furthermore, whereas acute stimulation of PKA (2–4 h) increases spine density, prolonged PKA stimulation (48 h) reduces spine density in apical dendrites of CA1 pyramidal neurons in organotypic slice cultures. The data from the AKAP150 mutant mice show that AKAP150-anchored PKA chronically limits the number of spines with functional AMPARs at 2–4 weeks of age. However, synaptic transmission and spine density was normal at 8 weeks in KO and D36 mice. Thus AKAP150-independent mechanisms correct the aberrantly high number of active spines in juvenile AKAP150 KO and D36 mice during development.

Dendritic spines receive most of the excitatory input in mammalian neurons (1, 2) and compartmentalize signaling that regulates the synaptic response (3, 4). Several protein kinases and phosphatases, including CaMKII, cAMP-dependent protein kinase (PKA),[3] PKC, and protein phosphatase PP2A and PP2B (calcineurin) (5) play prominent roles in synaptic plasticity. Synaptic activity translates into their activation, thereby affecting spine stability, morphology, and postsynaptic responses (6–13). Spines are dynamically gained and lost during synaptogenesis (9, 14–16) and in response to neuronal activity (17–19).

AKAP150 is a product of the *Akap5* gene in mice and is the main AKAP that recruits PKA to postsynaptic sites (20–25). It binds with its very C terminus to the N-terminal dimerization domain of the regulatory RII subunits of PKA (26, 27). It also binds PKC (28), PP2B (29, 30), and the SH3-GK region of the postsynaptic scaffolding proteins SAP97 and PSD-95 (31, 32). PSD-95 binds with its PDZ domains to the C-terminal ((S/T)*X*(I/V)) motif of NMDA-type glutamate receptor (NMDAR) NR2 subunits (33). PSD-95 also binds to the C terminus of stargazin (γ2) and its homologues γ3, γ4, and γ8, which associate with AMPAR-type glutamate receptor (AMPAR) for postsynaptic localization in conjunction with PSD-95 (34–36). SAP97 directly binds to the AMPAR GluR1 subunit via a PDZ-C-terminal interaction (37) to link AKAP150 and thereby PKA, PKC, and PP2B to GluR1 (38–41). Phosphorylation of GluR1 on Ser-845 by PKA can increase channel activity (42) and accumulation of GluR1-containing AMPAR at the postsynaptic site during hippocampal LTP (43, 44) (see also Refs. 45, 46). The N terminus of AKAP150 also binds F-actin, cadherin, adenylyl cyclases, and PIP_2 and targets AKAP150 to dendritic spines and the central region binds PSD-95 and its homologues (20, 47–51).

Bridging AMPAR, NMDAR, F-actin, PKA, PKC, and PP2B at spines, AKAP150 is an attractive candidate for correlating synaptic activity with spine morphology. We previously generated AKAP150 KO mice and mice that lack the PKA binding site at the C terminus of AKAP150 (D36 mice) (22, 25, 52). We showed earlier that PKA and its anchoring by AKAP150 plays an important role in LTP at an age of 2–3 weeks and again from 8 weeks on but not during 3–6 weeks (22). We found later that

* This work was supported, in whole or in part, by Grants DA015916, GM032875 (to G. S. M.), NS043254, NS056244, NS057714 (to S. S.), DC002961 (to S. H. G.), and NS035563, NS017502 (to J. W. H.) from the National Institutes of Health. This work was also supported by Grant 0655764Z (to M. E. D.) from the American Heart Association, startup funds from the University of South Alabama (to X. M. Z.), and the Intramural Research Program of the Eunice Kennedy Shriver National Institute of Child Health and Human Development, National Institutes of Health.

[1] To whom correspondence may be addressed: Building 10, Magnuson Clinical Center, 7D38, 10 Center Dr., Bethesda, MD 20892. E-mail: luyuan@mail.nih.gov.

[2] To whom correspondence may be addressed: 451 E. Health Sciences Dr., Davis, CA 95616-8636. Tel.: 530-752-6540; Fax: 530-752-7710; E-mail: jwhell@ucdavis.edu.

[3] The abbreviations used are: PKA, cAMP-dependent kinase; cpt-cAMP, 8-(4-chlorophenylthio)adenosine-cAMP; mEPSC, miniature excitatory postsynaptic currents; mIPSCs, miniature inhibitory postsynaptic currents; N6BnzcAMP, *N*6-benzoyladenosine-cAMP; KO, knockout; AKAP, a kinase anchor protein.

PKA activity and anchoring is required during LTD induction (23). Because LTP and LTD are both impaired in D36 mice rather than affected in an opposite manner, PKA must act via different molecular pathways in LTP and LTD. More recently we found that LTP is actually not impaired in AKAP150 KO mice in contrast to D36 mice (see "Discussion") and that D36 but not KO mice have impaired reversal learning of operant conditioning (25). Despite these different phenotypes we now report that both mouse strains show an increase in mEPSC frequency and linear spine density at 2–4 but not 8 weeks of age, suggesting that PKA anchoring is the most critical function of AKAP150 in controlling spine formation or maintenance. In support of a role of PKA in limiting spine density, chronic (48 h) activation of PKA reduced the density in organotypic hippocampal slice cultures whereas short term activation (2 h) had the opposite effect.

EXPERIMENTAL PROCEDURES

Animals—All animal procedures had been approved by the University of Iowa, the University of South Alabama, and the National Institute of Child Health and Human Development Animal Care and Use Committees and followed NIH guidelines. AKAP150 KO and D36 mouse strains were generated as previously described (22, 25, 52). Briefly, the entire coding sequence of the AKAP150 (*Akap5*) gene (GenBank™ locus XM138063 position 2126–2131) was replaced with a neomycin phosphotransferase cassette in AKAP150 KO mice by homologous recombination in embryonic stem cells in a 129S1/SvImJ background (Jackson Laboratories, Bar Harbor, ME). Mice were backcrossed 8 times with WT C57BL/6 (Taconic Farms Inc., Germantown, NY) to breed a nominally >99% genetic C57BL/6 background prior to study. For genotyping, DNA strands were isolated from supernatants of RNase A and proteinase K digested tail clips and used to amplify the 5′ coding region of AKAP150. The primers 5′-ATGGAGACCAGCGTTTCTGAG-3′ and 5′-TTCTGCTTCTTTGCAGGCACGG-3′ correspond to sequences upstream and downstream of a 290 bp fragment within AKAP150. The primers 5′-TCGCATGATTGAACAAGATGG-3′ and 5′-AAGCACGAGGAAGCGGTCAGC-3′ correspond to the sequences upstream and downstream of a 730 bp fragment within the neomycin cassette engineered into the mutant gene. WT mice show only the 290 bp band, KO mice only the 730 bp band, and heterozygous mice both bands.

To obtain AKAP150 D36 mice (22), in which the C-terminal most 36 residues were deleted, we had created a stop codon at the corresponding location in the AKAP150 gene. A neomycin resistance gene used for positive selection was flanked by loxP sites and removed by crossing the first generation of mutants to MEOX-cre mice. Mice were back-crossed >10 times with WT C57BL/6 (Taconic Farms) for a nominally >99% genetic C57BL/6 background. DNA (tail clips) was used to amplify the region by PCR using primers that corresponded to sequences upstream and downstream of the newly created stop codon (5′-CCCACAGATACAGAGAAACCGAG-3′ and 5′-GGAAACGAAGTCACTGGAACAGCG-3′). The 400 bp product was purified and digested with XbaI to test for the XbaI restriction site that had been created by the newly engineered stop codon. DNA with the engineered stop codon showed cleavage products of 285 bp and 115 bp.

Recording of mEPSCs, mIPSCs, and AMPAR EPSC/NMDAR EPSC Ratio—All mice were decapitated with an appropriate guillotine without anesthesia before collection of brains and production of hippocampal slices as approved by the University of Iowa Animal Care and Use Committee following NIH guidelines. Acute hippocampal slices were prepared as described exclusively from male mice (22). Briefly, transverse brain slices (350 μm thick) were prepared with a vibrating microtome (VT1000S, Leica Microsystems, Nussloch, Germany), under ice-cold artificial cerebrospinal fluid (ACSF; in mM: 127 NaCl, 26 $NaHCO_3$, 1.2 KH_2PO_4, 1.9 KCl, 2.2 $CaCl_2$, 1 $MgSO_4$, 10 dextrose) saturated with 95% O_2 and 5% CO_2. Slices were kept in oxygenated ACSF for at least 1 h before transfer to a submersion-type recording chamber, which was continually perfused with oxygenated ACSF (2 ml/min, 32 °C). AMPAR-mediated mEPSCs were recorded from CA1 pyramidal neurons in whole-cell patch configuration with a holding potential at −70 mV (22). Patch pipettes (3–6 MΩ) were filled with internal solution (in mM: 125 K-gluconate, 20 KCl, 10 NaCl, 2 Mg-ATP, 0.3 Na-GTP, 2.5 QX314, 10 PIPES, 0.2 EGTA, pH 7.3 with KOH). $GABA_A$ receptor currents were blocked with 50 μM picrotoxin (Sigma), NMDAR currents with 10 μM APV (Sigma), and Na^+ channel currents with 1 μM tetrodotoxin (TTX, Sigma). Miniature inhibitory postsynaptic currents (mIPSCs) were recorded from CA1 pyramidal neurons in whole-cell patch configuration with a holding potential at −70 mV. Patch pipette were filled with internal solution (in mM: 140 CsCl, 1 EGTA, 10 HEPES, 3.6 NaCl, 2 Mg-ATP, 0.4 Na-GTP, 5 QX314). AMPAR currents were blocked with 40 μM DNQX, NMDAR currents with 10 μM APV (Sigma), and Na^+ channel currents with 1 μM tetrodotoxin (TTX, Sigma). Mini IPSCs were completely blocked by bicuculline (10 μM) at the end of recording. To get AMPAR EPSC to NMDAR EPSC ratio, EPSCs were recorded from CA1 pyramidal neurons in whole-cell patch configuration with a holding potential at −70 mV or +50 mV. Patch pipettes (3–6 MΩ) were filled with internal solution (in mM: 125 Cs-gluconate, 20 CsCl, 10 NaCl, 2 Mg-ATP, 0.3 Na-GTP, 2.5 QX314, 10 PIPES, 0.2 EGTA, pH 7.3 with KOH). 10 μM gabazine was bath-applied to inhibit $GAGA_A$ current. Peak amplitude of ESPCs at −70 mV was measured as AMPAR-mediated currents. Amplitude of EPSCs at 70 ms after onset of EPSCs at +50 mV was measured as NMDAR-mediated currents. Recordings were performed with an Axopatch 200B amplifier (mEPSC, mIPSC) or a Multiclamp700B amplifier, filtered at 1 kHz, and digitized at 10 kHz via an Axon Digidata 1322A. The threshold for accepting events as mEPSCs and mIPSCs was defined as 5 pA.

DiOlistic Labeling of Fixed Hippocampal Slices—Male mice aged 2, 4, or 8 weeks old were deeply anesthetized with a mixture of ketamine and xylazine as approved by the University of Iowa Animal Care and Use Committee following NIH guidelines. Mice were transcardially perfused first with 20 ml of PBS to wash out blood in vessels and then with 20 ml of 4% paraformaldehyde (PFA) in 0.1 M phosphate buffer (PB, in mM: 80 Na_2HPO_4, 20 NaH_2PO_4, pH 7.4) for fixation. Brains were removed, post fixed (1 h, 4% PFA in 0.1 M PB), rinsed with PBS 3 times, glued onto the plateau of the slicing chamber, and

immersed into PBS. Transverse slices (300 μm thick) were prepared with a vibrating microtome (VT1000S as above) and stored in PBS containing 0.02% NaN_3 before labeling. Tungsten particles were coated with the long chain lipophilic fluorescent dye 1,1′-dioctadecyl-3,3,3′,3′-tetramethylindo-carbocyanine perchlorate (DiI) following the method in Ref. 53. Briefly, ~2 mg of DiI (D-282; Molecular Probes) was dissolved in 200 μl of methylene chloride. Tungsten particles (50 mg; 1.0 μm diameter; Bio-Rad) were placed on a glass slide. The dissolved dye was added to the tungsten, spread around the glass slide and allowed to dry. The DiI-coated tungsten particles were scraped into a vial and mixed with 3 ml of distilled water to obtain a homogenous solution. The solution was loaded into polyethylene tubing (diameter: ~2 mm) and allowed to adhere. The water was removed from the tubing leaving behind a lining of DiI-coated tungsten. The tubing was air-dried for 10 min and cut into 13-mm long pieces. Cortical pyramidal neurons were labeled by shooting the DiI micro-tungsten particles into the fixed hippocampal slices with a Helios Gene Gun (Bio-Rad). Slices were immersed in PBS and placed into a 37 °C incubator where the DiI was allowed to incorporate into the neuronal membrane for 24 h. A Bio-Rad Radience 2100MP Multiphoton/Confocal Microscope was used to image the labeled structures. Specimens were excited with green HeNe laser providing the laser line of 543 nm, and emission was collected at the wavelength of 568 nm. A stack of images at 0.5 μm steps was acquired. Spine density was determined by manually counting spines along 40–60 μm-long dendritic segments switching to neighboring optical plane sections to follow the dendrites as the dendrites proceed into the corresponding regions. The experimenter determining spine density was blind with respect to the genotype.

Hippocampal Slice Culture and Biolistic Transfection—Rat and mouse hippocampal organotypic slice cultures were prepared as described earlier (54, 55). Briefly, rats were euthanized by rapid decapitation following cold narcolepsy. Hippocampi from postnatal day 6–7 (P6-P7) rats were dissected and cut into 300 μm thick transverse slices using a manual tissue chopper. Slices were placed in Falcon polyethylene terephthalate-etched membrane culture inserts containing 1 mm pores (Fisher). Slices were maintained in filter culture medium (FCM; 25% horse serum, 25% Hanks Balanced Salt Solution, 50% MEM, 2 mM glutamine, 44 mg/ml $NaHCO_3$, and 10 units/ml penicillin-streptomycin). Slices were grown in a 5% CO_2 humidified incubator. The medium was changed every 2–3 days. Biolistic transfection of slice cultures was done using a Helios Gene Gun (Bio-Rad), as previously described (56). For spine analysis, P6 rats were cultured for 5 days, or P7 rats were cultured for 4 to 5 days before transfection of GFP-tagged PSD-95-GFP or -YFP or Lck-GFP. Various drugs were added either on the day of transfection (48 h time points) or later for shorter incubations.

Comparisons among culture conditions were performed on slices dissected and cultured in parallel at the same time. For counting spine PSDs, slices were fixed with 4% PFA in PBS 48 h after transfection. Images were captured using a Leica SP2 AOBS confocal microscope. Illumination was provided by Ar and green He-Ne lasers. For analysis of spines and synapses in fixed tissues, a series of high-resolution images (1024 × 1024 pixel array) was captured at a z-step of 0.6–0.8 μm using a 63x/1.2 NA APO water-immersion objective with an additional electronic zoom of 2.83. Each captured image was an average of 3–4 scans in a single plane. For each transfected neuron, one 100-μm segment of an apical dendrite (starting ~50 μm from the soma in *S. radiatum*) was imaged for spine and synapse analysis. With the conditions we used for biolistic transfection, only a few (usually 1–4) neurons per slice were transfected and overlap of dendritic arbors was rare. This approach allowed us to distinguish individual neurons and dendrite segments clearly without interference from other labeled cells. Dendrites were not scored in those few cases when transfected neurons were clustered and dendrites overlapped. Quantification of PSD and spine density was done as described earlier (55), with the observer blinded to the experimental conditions and/or genotypes of the animals.

Statistical Analysis—Statistical analysis was performed with GraphPad Prism software. Results are shown as mean ± S.E. Two-tailed Student's *t* test or Mann-Whitney test was performed depending on the normality of distributions. One-way ANOVA followed by Bonferroni's multiple comparison tests was performed in cases of multiple comparisons. *p* values are indicated in figures or figure legends.

RESULTS

Increased mEPSC Frequency and Spine Density in AKAP150 KO Mice at 2 and 4 but Not 8 Weeks of Age—Earlier evidence suggests that PKA could regulate spine density (57) (see below). To investigate if AKAP150 KO mice have altered synaptic density we first monitored AMPAR-mediated mEPSCs frequency from CA1 pyramidal neurons. In fact, the mEPSC frequency was increased by 53 and 33% in 2- and 4-week-old AKAP150 KO mice, respectively, compared with littermate WT (Fig. 1). However, at 8 weeks, mEPSCs frequency was normal in KO mice. Neither amplitude nor decay time constant (decay tau) of AMPAR-mEPSCs was changed in 2-, 4-, and 8-week-old AKAP150 KO mice (Fig. 1). Individual synapses thus appear normal with respect to basal synaptic transmission.

Increased mEPSC frequency could be due to increased frequency of spontaneous pre-synaptic vesicle release or increased number of synapses. Alterations in presynaptic glutamate release are typically obvious by changes in paired-pulse facilitation (PPF) (58–61). PPF was normal in AKAP150 KO mice at all ages (Fig. 1) suggesting normal presynaptic function. To test whether synapse density was increased in the younger KO mice, we DiOlistically labeled hippocampal neurons in 2-, 4-, and 8-week-old mice and determined the linear density of dendritic spines, which constitute the postsynaptic sites of glutamatergic synapses on pyramidal neurons. Spine density was increased at 2 and 4 weeks (by 28 and 10% in KO) but not at 8 weeks (Fig. 2). At the same time, neither spine head size, nor spine length, nor dendritic diameter was altered at any age.

Increased mEPSC Frequency and Spine Density in AKAP150 D36 Mice at 2–4 but Not 8 Weeks of Age—Because AKAP150 has multiple binding partners we performed a thorough analysis of mEPSC properties and spine density in D36 mice to more specifically define whether the alterations in KO mice are due to loss of PKA anchoring. Similar to KO, the mEPSC frequency

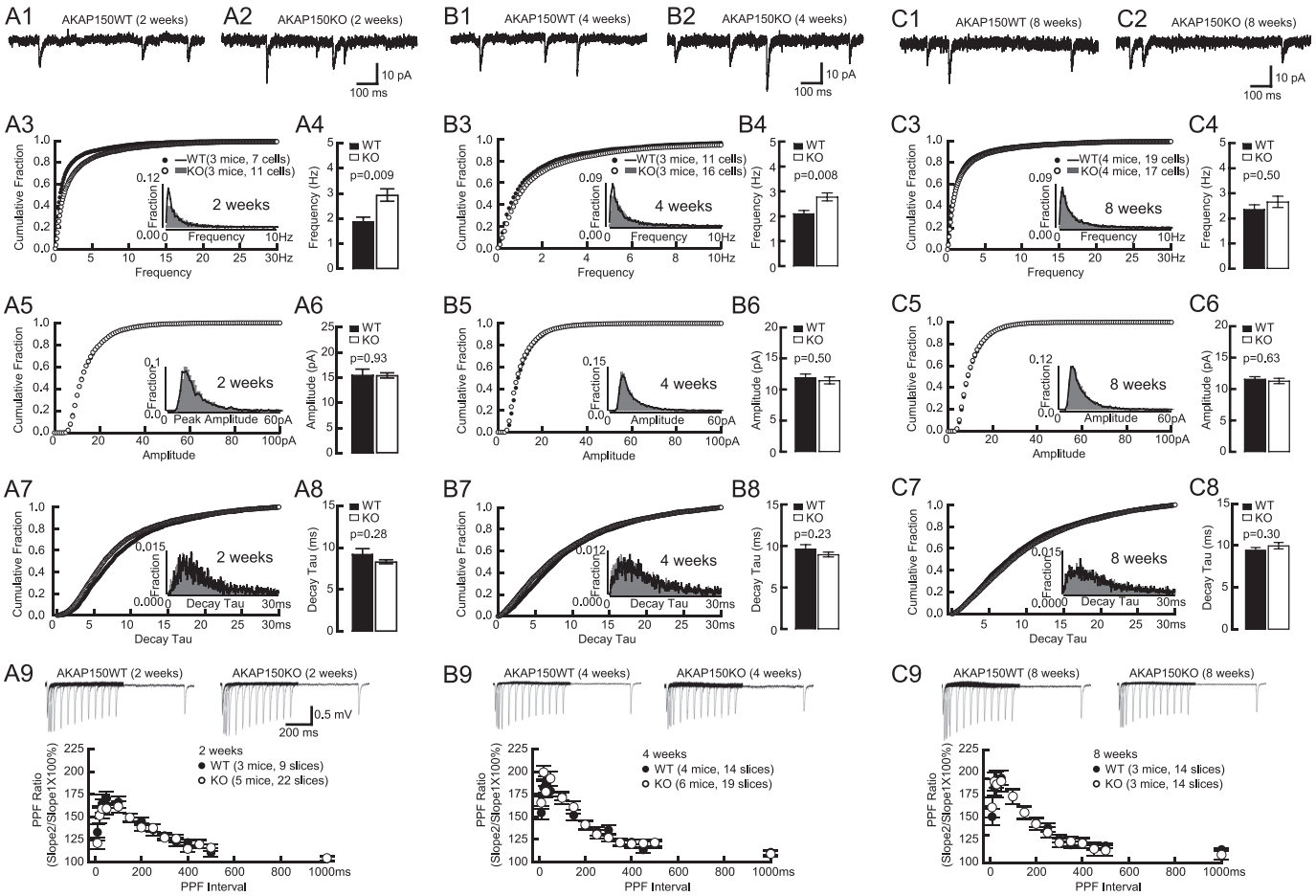

FIGURE 1. **mEPSC and PPF in AKAP150 KO mice.** *Top panels* are examples of AMPAR mEPSCs from acute hippocampal slices from littermate WT and KO mice of 2 weeks (*A1, A2*), 4 weeks (*B1, B2*), and 8 weeks (*C1, C2*). Cumulative fraction (*A3, B3*) and histogram distribution (*inset*) of mEPSC frequency show a right shift, and the frequency averages (*A4, B4*) are significantly increased in 2-week-old KO (2.9 ± 0.2Hz) *versus* WT (1.9 ± 0.2Hz; $p < 0.01$), and 4-week-old KO (2.8 ± 0.2 Hz) *versus* WT (2.1 ± 0.1 Hz; $p < 0.01$) but are not affected in 8-week-old KO (2.7 ± 0.2 Hz) *versus* WT (2.4 ± 0.2 Hz) mice (*C3, C4*). Cumulative fractions and histogram distribution (*insets*) of mEPSC amplitudes are not affected in KO at 2 (*A5*), 4 (*B5*), and 8 weeks (*C5*). The amplitude averages are comparable between KO and littermate WT at 2 weeks (KO, 15.4 ± 0.5pA *versus* WT, 15.5 ± 1.2pA; *A6*), 4 weeks (KO, 11.4 ± 0.6 pA *versus* WT, 11.9 ± 0.6 pA; *B6*), and 8 weeks (KO, 11.3 ± 0.4 pA *versus* WT, 11.6 ± 0.4 pA; *C6*). Cumulative fractions and histogram distribution (*insets*) of mEPSC decay tau are not affected in KO at 2 (*A7*), 4 (*B7*), and 8 weeks (*C7*). The decay tau averages are comparable between KO and littermate WT at 2 weeks (KO, 8.3 ± 0.2 ms *versus* WT, 9.2 ± 0.7 ms; *A8*), 4 weeks (KO, 9.0 ± 0.3 ms *versus* WT, 9.6 ± 0.5 ms; *B8*), and 8 weeks (KO, 10.0 ± 0.4 ms *versus* WT, 9.5 ± 0.3 ms; *C8*). PPF is normal in AKAP150 KO *versus* litter-matched WT mice that were 2 weeks (*A9*), 4 weeks (*B9*), or 8 weeks (*C9*) old. Inter-stimulus intervals ranged from 10–1000 ms. No statistically significant differences were obvious. Example PPF traces are shown in the *top panel* of *A9, B9*, and *C9*. *p* values of Mann-Whitney test are shown in each subpanel.

was increased at 4 weeks (by 48%) but not 8 weeks of age whereas the mEPSC amplitude and decay tau were unchanged at both ages (Fig. 3). We found earlier that the overall strength of postsynaptic AMPAR responses is normal as determined by fEPSP recordings at 2–8 weeks with respect to input/output relationships as well as PPF (22, 23). DiOlistical labeling of hippocampal sections from 2-, 4-, and 8-week-old mice showed that the linear spine density was increased at 2 and 4 weeks by 48 and 17% in D36, respectively, but not at 8 weeks (Fig. 4). However, neither spine head size, nor spine length, nor dendritic diameter was altered at any age.

Ratio of AMPAR-EPSC to NMDAR-EPSC Is Increased in Young D36 Mice—The increase in spine density is about half of the increase in mEPSC frequency for KO at 2 and 4 weeks and for D36 at 4 weeks. We thus measured the magnitude of postsynaptic AMPAR- and NMDAR-mediated responses upon stimulation of synaptic transmission in young (2–3-week-old) mice (Fig. 5). It appeared that AMPAR-mediated evoked EPSCs were increased in KO and D36 compared with WT mice whereas NMDAR-mediated evoked EPSCs appeared largely unaffected. In support of these observations, the average of the ratios of AMPAR/NMDAR EPSCs from individual neurons was increased by ~38% for both genotypes (Fig. 5). This change in ratio is consistent with the notion that a larger portion, perhaps the majority, of the additional population of synapses in KO and D36 mice might contain functional AMPARs than the synapse population in WT. In other words, the overall portion of silent synapses (those containing functional NMDAR but not AMPAR) is lower in mutant than WT mice. Thus the combination of increases in spine density and synapses with AMPAR accounts for the more substantial increase in mEPSC frequency compared with the less dramatic increase in spine density.

Postsynaptic PKA Activity Regulates Spine Density in Slice Cultures—To further characterize the role of PKA in controlling spine density, we biolistically transfected organotypic hippocampal slice cultures with PSD-targeted PSD-95-GFP or PSD-95-YFP constructs (Fig. 6) or the more generally membrane-directed Lck-GFP construct (62) (Fig. 7) and maintained

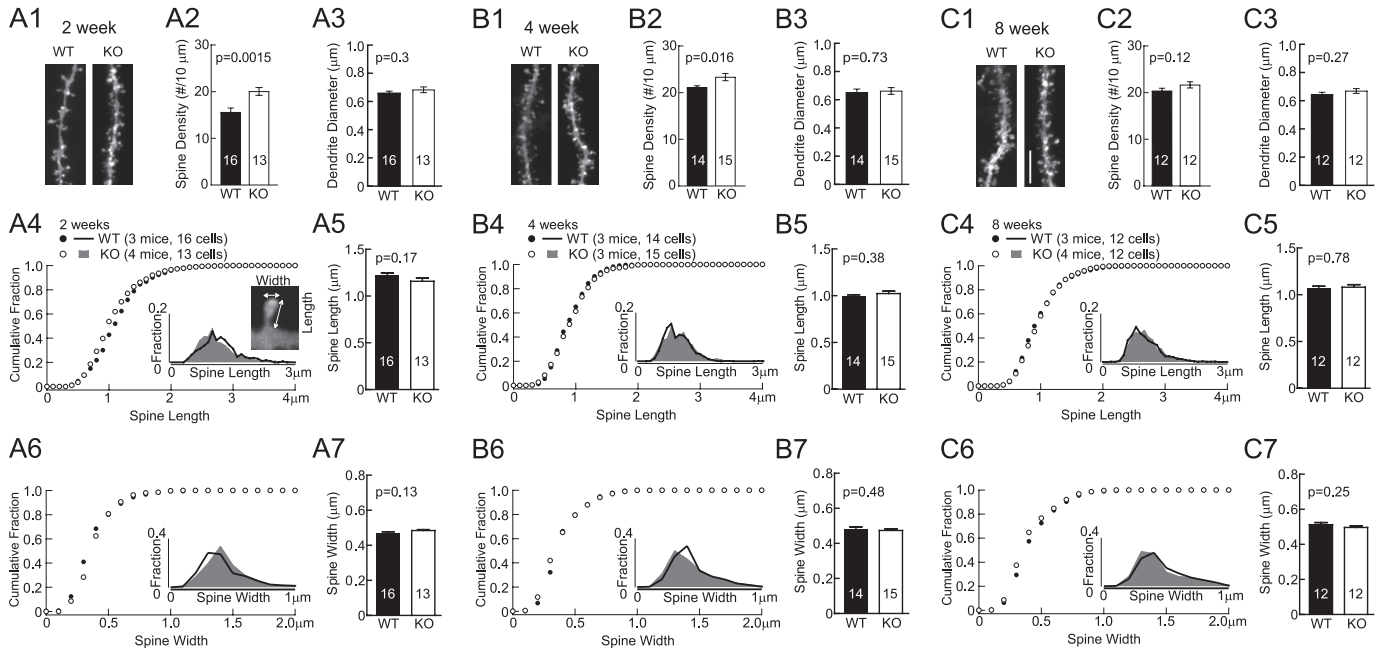

FIGURE 2. **Increase in spine density in AKAP150 KO mice *versus* littermate wt controls.** Representative images of apical dendrites and spines of CA1 pyramidal neurons in mice perfused at 2, 4, and 8 weeks are shown in *A1*, *B1*, and *C1* respectively (scale bars, 5 μm). Spine density is increased by 28% in KO (20 $\pm$ 0.8/10 μm) *versus* WT (15.6 $\pm$ 0.9/10 μm) at 2 weeks (*A2*) and by 10% in KO (23.3 $\pm$ 0.8/10 μm) *versus* WT (21.1 $\pm$ 0.4/10 μm) at 4 weeks (*B2*); it is comparable in KO (21.7 $\pm$ 0.7/10 μm) and WT (20.3 $\pm$ 0.6/10 μm) at 8 weeks (*C2*). Dendrite diameters are comparable between KO and WT control at 2 weeks (KO, 0.68 $\pm$ 0.02 μm; WT, 0.66 $\pm$ 0.02 μm; *A3*), 4 weeks (KO, 0.66 $\pm$ 0.02 μm; WT, 0.65 $\pm$ 0.02 μm; *B3*), and 8 weeks (KO, 0.67 $\pm$ 0.02 μm; WT, 0.65 $\pm$ 0.02 μm; *C3*). Cumulative fractions and histogram distributions (*insets*) of spine length and head width are unchanged in KO at 2 weeks (*A4*, *A6*), 4 weeks (*B4*, *B6*), and 8 weeks (*C4*, *C6*). Spine length and head width averages are comparable for KO and WT littermates of 2 weeks (*A5*, KO length, 1.16 $\pm$ 0.03 μm *versus* WT length, 1.23 $\pm$ 0.02 μm; *A7*, KO width, 0.48 $\pm$ 0.01 μm *versus* WT width, 0.47 $\pm$ 0.01 μm), 4 weeks (*B5*, KO length, 1.02 $\pm$ 0.02 μm *versus* WT length, 1.00 $\pm$ 0.01 μm; *B7*, KO width, 0.47 $\pm$ 0.01 μm *versus* WT width, 0.48 $\pm$ 0.01 μm), and 8 weeks (*C5*, KO length, 1.08 $\pm$ 0.02 μm *versus* WT length, 1.07 $\pm$ 0.02 μm; *C7*, KO width, 0.50 $\pm$ 0.01 μm *versus* WT width, 0.51 $\pm$ 0.01 μm). *p* values of Student's *t*-tests are shown in each subpanel.

the slices in culture for 2 more days. PKA modulators were applied for 2 or 48 h before fixation and quantification of GFP/YFP-labeled spines in apical dendrites of CA1 pyramidal neurons. Similar to earlier reports (*e.g.* Ref. 63) we found that spine density was lower in our organotypic hippocampal slice cultures after 5–6 DIV as compared with perfused mouse brain at 2, 4, and 8 weeks of age by a factor of 4–5. This low spine density is likely at least in part due to differences in the actual developmental stages of organotypic slice cultures *versus in vivo* as it increases strongly after 3–4 weeks in culture (63). This observation also illustrates the importance of the analysis of spine density in perfused brain, which reflects the actual *in vivo* situation, and of the analysis of synaptic transmission in acute hippocampal slices, as described above.

In the organotypic slice cultures the structurally and functionally different PKA inhibitors H-89 and 11R-PKI (the inhibitory PKI peptide tagged with 11 Arg for membrane permeability (22)) increased spine density over 48 h as determined with the PSD-95-GFP (Fig. 6*A*, *left*) and PSD-95-YFP probes (Fig. 6*A*, *right*), respectively. 11R-PKI as well as a third unrelated PKA inhibitor, Rp-cAMPS, showed the same effect, *i.e.* increased spine density over a 48 h period with Lck-GFP as cell surface label (Fig. 7*A*). Strikingly, when applied for 2 h the latter two PKA inhibitors had the opposite effect, *i.e.* they decreased spine density (Fig. 7*A*). The PKA activators Sp-cAMPS, N6BnzcAMP and 8-cpt-cAMP had the exact opposite effects as compared with the inhibitors: spine density of hippocampal slice cultures was decreased after 48 h treatments with 8-cpt-cAMP (Fig. 6*A*) or Sp-cAMPS (Fig. 7*A*), whereas spine density was increased after 2 h treatments with Sp-cAMPS or N6BnzcAMP (Fig. 7*A*). Spine width and length and dendrite diameter remained unaffected under any condition illustrated in Fig. 7*A*.

A more detailed time course as determined in a completely new set of experiments showed that SpcAMPS significantly increased spine density when applied for 2–4 h, has no statistically significant effect over 10–24 h, and significantly decreases density after 48 h and that RpcAMPS causes exactly the reverse effects (Fig. 8). To test whether changes were due to pre- or post-synaptic effects, the endogenous PKA inhibitor PKI was fused to CFP and cotransfected with PSD-95-YFP, which increased spine density by 25% (Fig. 6*A*). As biolistic transfection efficiency is so low that synaptic contacts between transfected neurons are not observed, we conclude that chronic postsynaptic PKA inhibition up-regulates synaptic density in a cell-autonomous manner.

Role of PP2A in Controlling Spine Density—The positive effect of PKA activation for 1–2 h on spine density and size has been noted previously and ascribed to PKA counteracting inhibition of the negative effect of Cdk5 on WAVE1-controlled F-actin polymerization (57) and to PKA regulating Rap1 via GTPase activating Rap1GAP and perhaps via direct phosphorylation (see Ref. 64 and references therein). The molecular details of the negative effect of chronic inhibition of PKA activity and anchoring are new and completely unclear. The Ser/Thr phosphatase PP2A (65) has been linked to LTD, which in turn

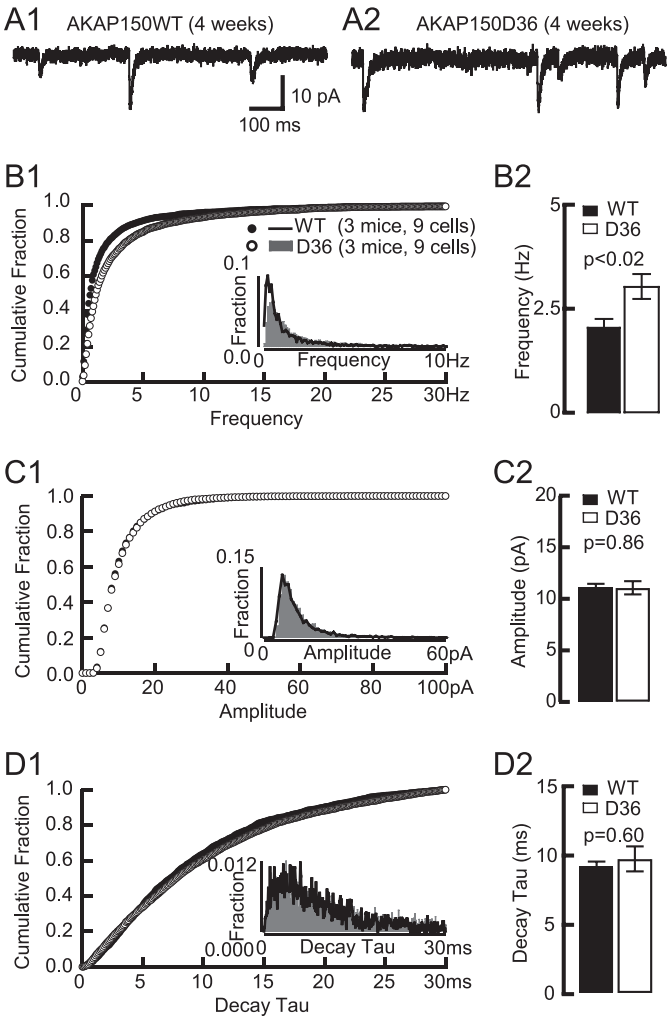

FIGURE 3. **AMPAR mEPSC in 4-week-old D36 mice.** *A*, examples of AMPAR mEPSCs from acute hippocampal slices from 4-week-old litter mate WT (*A1*) and D36 mice (*A2*). Cumulative fraction (*B1*) and histogram distribution (*inset*) of mEPSC frequency show a right shift and the frequency averages (*B2*) are dramatically increased in 4-week-old D36 (3.1 ± 0.3 Hz) *versus* WT mice (2.1 ± 0.2 Hz; $p < 0.02$). Cumulative fraction (*C1*) and histogram distribution (*inset*) of mEPSC amplitude are unchanged in 4-week-old D36. The amplitude average (*C2*) is comparable between D36 (11.1 ± 0.6 pA) and littermate-matched WT (11.1 ± 0.3 pA). Cumulative fraction (*D1*) and histogram distribution (insert) of mEPSC decay tau is not significantly changed in 4-week-old D36. The decay tau average (*D2*) is comparable between D36 (9.6 ± 0.9 ms) and WT (9.1 ± 0.3 ms). *p* values of Mann-Whitney test are shown in each subpanel.

correlates with spine shrinkage and loss (66, 67). Furthermore, PP2A holoenzymes that contain the B'δ (B56δ) subunit are activated by PKA (68). Because inhibition of PP2A counteracts LTD (65) this pathway appeared plausible for the spine reducing effect of PKA. However, 48 h treatment with 1 nM okadaic acid (OA), which specifically inhibits PP2A at such low concentration, did not affect spine density (Fig. 8). If chronic inhibition of basal PKA activity would work by reducing basal PP2A/B'δ activity, spine density should have been increased. Accordingly, basal PKA activity, which keeps spine number in check, does not act via PP2A in general. However, 1 nM OA did prevent the decrease in spine density by 48 h treatment with SpcAMPS. These results suggest that basal PKA activity does not curb spine density via PP2A but the additional spine loss by chronically stimulated PKA activity does require PP2A.

Role of Different AKAP150 Domains in Regulating Spine Density in Slice Cultures—To define which regions of AKAP150 are critical for regulating spine density by PKA we co-transfected WT slice cultures with Lck-GFP and various constructs derived from AKAP79 (50), the human homolog of AKAP150, which is lacking an insert of 36 octapeptide repeats of unknown functions and thereby likely a better choice for defining the relevant domains. Overexpression of full-length AKAP79 (residues 1–427), N terminus (1–153), and N- plus C terminus (Δ109–315 lacking the central region) had no effect but residues 1–361, which are only lacking the PKA binding site, increased spine density after 48 h (Fig. 7*B*). Thus residues 1–361 act in a dominant negative fashion but residues 1–153, which bind F-actin, cadherin, adenylyl cyclase, and PIP_2, and mediate AKAP79/150 targeting, do not. Accordingly, the dominant negative effect of constructs that lack PKA binding requires the central domain (residues 153–315), which binds PSD-95 and its homologues (50), presumably because this interaction is important for postsynaptic localization of AKAP150.

As expected, spine density was also increased in slice cultures from D36 *versus* WT mice (Fig. 6*B*). This increase was converted or rescued back to WT spine density by biolistic transfection of individual neurons with full length AKAP79 (Fig. 7*C*). Accordingly, the increased spine density in young D36 mice is not due to irreversible developmental defects that would have become independent of AKAP150 and its anchoring of PKA. As the number of transfected neurons is very low, these results provide further indication that the suppression of spine density by AKAP150-anchored PKA is cell autonomous and postsynaptic in nature consistent with the PKI-CFP effect (Fig. 6*A*). Finally, addition of the PKA inhibitors 11R-PKI and RpcAMPS for 48 h did not further increase spine density in D36 slices. Thus, in contrast to WT slices, basal PKA activity no longer curbs spine density in D36 slices as it is displaced from AKAP150-containing signaling complexes.

Frequency of mIPSCs Is Increased in AKAP150 D36 and KO Mice—Increased excitatory neurotransmission is often accompanied by alterations in inhibitory transmission (69). In 2-week-old AKAP150 KO and D36 mice, both frequency as well as amplitude of mIPSCs are increased without a detectable change in the decay time constant (Fig. 9). Accordingly, both the number and strength of spontaneously active inhibitory synapses are up-regulated in the mutant mice, possibly to counteract the increase in the number of spontaneously active excitatory synapses in these mice for maintenance of homeostasis of neuronal activity (69).

DISCUSSION

We provide electrophysiological and histological evidence that AKAP150-anchored PKA negatively regulates formation or maintenance of dendritic spines. The increase in AMPAR mEPSCs frequency in CA1 pyramidal neurons in young AKAP150 mutant mice is due to a larger number of *de facto* rather than detectable events, because mEPSC amplitude and decay time constant averages and fractional distributions are not affected. In other words, the increase in frequency is not due to an increase in amplitude, which could otherwise move some small mEPSC events out of the electric noise. Moreover,

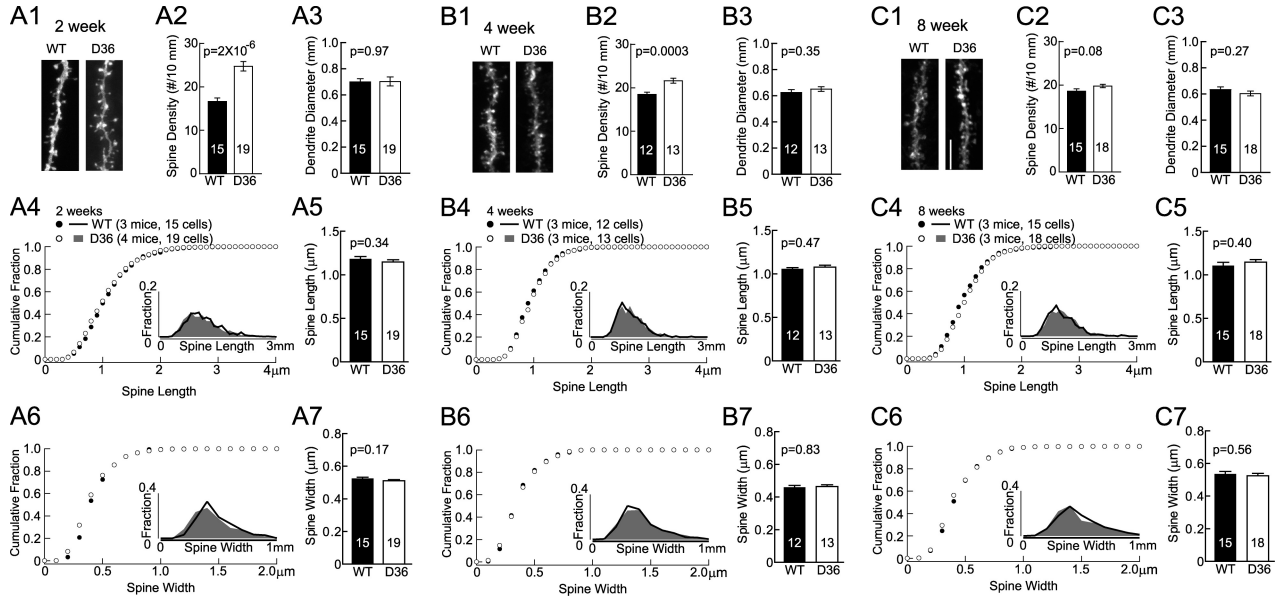

FIGURE 4. **Increase in spine density in AKAP150 D36 mice *versus* litter mate wt controls.** Representative images of apical dendrites and spines of CA1 pyramidal neurons in mice perfused at 2, 4, and 8 weeks are shown in *A1*, *B1*, and *C1* respectively (scale bars, 5 μm). Spine density is increased by 48% in D36 mice (24.6 $\pm$ 1.1/10 μm) *versus* WT (16.6 $\pm$ 0.8/10 μm) at 2 weeks (*A2*) and by 17% in D36 mice (21.5 $\pm$ 0.6/10 μm) *versus* WT (18.4 $\pm$ 0.5/10 μm) at 4 weeks (*B2*); it is comparable in D36 mice (19.7 $\pm$ 0.4/10 μm) *versus* WT (18.5 $\pm$ 0.5/10 μm) at 8 weeks (*C2*). Dendrite diameters are comparable between D36 and WT control at 2 weeks (D36, 0.7 $\pm$ 0.03 μm; WT, 0.7 $\pm$ 0.02 μm; *A3*), 4 weeks (D36, 0.65 $\pm$ 0.02 μm; WT, 0.62 $\pm$ 0.02 μm; *B3*), and 8 weeks (D36, 0.60 $\pm$ 0.02 μm; WT, 0.63 $\pm$ 0.02 μm; *C3*). Cumulative fractions and histogram distributions (*insets*) of spine length and head width are unchanged in D36 of 2 weeks (*A4, A6*), 4 weeks (*B4, B6*), and 8 weeks (*C4, C6*) old. Spine length and head width averages are comparable for D36 and WT littermates of 2 weeks (*A5*, D36 length, 1.15 $\pm$ 0.02 μm *versus* WT length, 1.18 $\pm$ 0.03 μm; *A7*, D36 width, 0.51 $\pm$ 0.01 μm *versus* WT width, 0.52 $\pm$ 0.01 μm, respectively), 4 weeks (*B5*, D36 length, 1.08 $\pm$ 0.02 μm *versus* WT length, 1.06 $\pm$ 0.02 μm; *B7*, D36 width, 0.46 $\pm$ 0.01 μm *versus* WT width, 0.46 $\pm$ 0.01 μm), and 8 weeks (*C5*, D36 length, 1.15 $\pm$ 0.03 μm *versus* WT length, 1.10 $\pm$ 0.04 μm; *C7*, D36 width, 0.52 $\pm$ 0.01 μm *versus* WT width, 0.54 $\pm$ 0.01 μm). *p* values of Student's *t*-tests are shown in each subpanel.

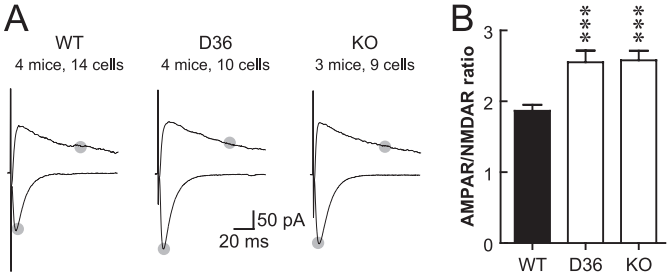

FIGURE 5. **Increase in the ratio of AMPAR- to NMDAR-mediated EPSCs in 3-week-old AKAP150 KO and D36 mice.** *A*, example traces of EPSC at -70 and $+50$ mV. *Gray dots* indicate the time points that were used to determine the magnitudes of EPSCs for AMPAR (*bottom*) and NMDAR (*top*). *B*, AMPAR/NMDAR EPSC ratio is increased in D36 (2.55 $\pm$ 0.16) and KO (2.58 $\pm$ 0.13) mice compared with WT controls (C57BL/6, 1.86 $\pm$ 0.08; one-way ANOVA, $p = 0.0002$; ***, post-hoc Bonferroni's multiple comparison with WT, $p < 0.001$).

changes in spine density and in AMPAR/NMDAR EPSC ratio follow the same age-dependent pattern as mEPSC frequency: both parameters are increased at 2–4 weeks but return to normal at 8 weeks of age (see Figs. 2 and 4 for spine density and Fig. 5 and Ref. 22 for AMPAR/NMDAR EPSC ratio).

The increase in spine density (28 and 10% in KO at 2 and 4 weeks, respectively, and 17% in D36 at 4 weeks) is significantly smaller than the increase in mEPSC frequency (53 and 33% in KO at 2 and 4 weeks, respectively, and 45% in D36 at 4 weeks). The increase in AMPAR/NMDAR EPSC ratio suggests that KO and D36 mice have a larger portion of synapses with functional AMPAR and thereby a smaller portion of silent synapses than WT. The increase in mEPSCs frequency and spine density is more dramatic in AKAP150 D36 than KO mice, possibly because other AKAPs substitute for AKAP150 in KO mice.

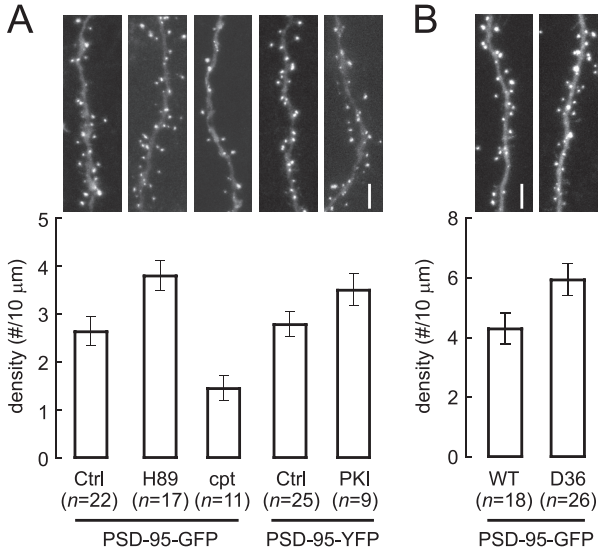

FIGURE 6. **Postsynaptic, AKAP150-anchored PKA regulates spine density of hippocampal CA1 pyramidal neurons as determined by PSD-95-GFP/YFP labeling.** Organotypic hippocampal slice cultures from P6–7 pups were transfected after 4–5 DIV with GFP-PSD-95 (*left* in *A*; *B*) or with PSD-95-YFP plus CFP-PKI (*right* in *A*). PSD-95-GFP-transfected slices were treated with 5 μM H-89 or 100 μM cpt-cAMP for 48 h, as indicated, before fixation. PSD-95-GFP/YFP puncta were counted in confocal images. *Top panels* show representative images. *A*, in WT slices, density of spine-localized PSDs was increased upon PKA inhibition by H-89 (3.8 $\pm$ 0.3/10 μm; $p < 0.05$, Bonferroni's multiple comparison following one-way ANOVA) or PKI transfection (3.5 $\pm$ 0.3/10 μm; $p < 0.05$, Student's *t* test) *versus* control (PSD-95-GFP, 2.6 $\pm$ 0.3/10 μm; and PSD-95-YFP, 2.8 $\pm$ 0.3/10 μm, respectively), and decreased by cpt-cAMP (1.4 $\pm$ 0.2/10 μm; $p < 0.01$, Bonferroni's multiple comparison following one-way ANOVA). *B*, transfection of cultured slices from D36 or WT mice with PSD-95-GFP reveals 37% increase in spine PSD density in D36 mice (5.9 $\pm$ 0.5/10 μm) *versus* WT (4.3 $\pm$ 0.5/10 μm, $p < 0.05$, Student's *t* test; *n:* number of neurons quantified).

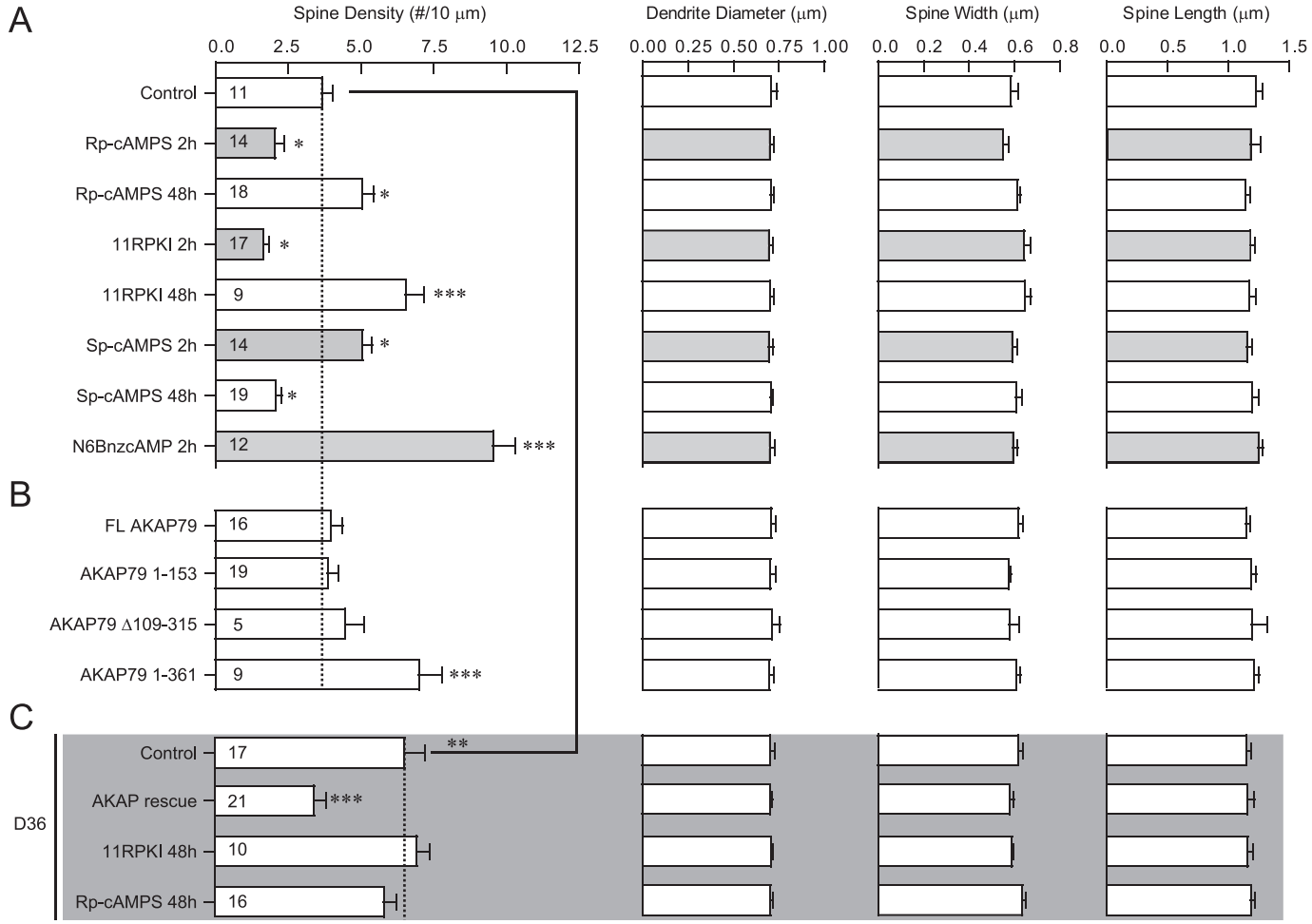

FIGURE 7. **Organotypic hippocampal slice cultures from P6-P7 WT (*A, B*) or D36 pups (*C*; gray background) were transfected after 4–5 DIV with Lck-GFP plus the indicated AKAP79 constructs.** Cultures were fixed after 48 h and spines analyzed from confocal images. Cultures were treated with 200 μM Rp-cAMPS or Sp-cAMPS, 10 μM 11R-PKI, 100 μM N6BnzcAMP, for 2 h (*gray bars*) or 48 h (*open bars*) before fixation, as indicated. (*n:* number of neurons quantified from a minimum of three independent experiments for each condition). Significance of effects on spine densities was determined by ANOVA followed by Bonferroni's multiple comparison test with WT control in *A* for *A* and *B* and indicated as: *, $p < 0.05$; **, $p < 0.01$; ***, $p < 0.0001$. Bonferronis' multiple comparison test with D36 control in *C* was also performed following ANOVA of spine density for conditions in *C* ($p < 0.0001$ for AKAP rescue). Spine density of D36 control (*C*) is significantly increased compared with WT control (*A*) ($p < 0.01$, Student's *t* test).

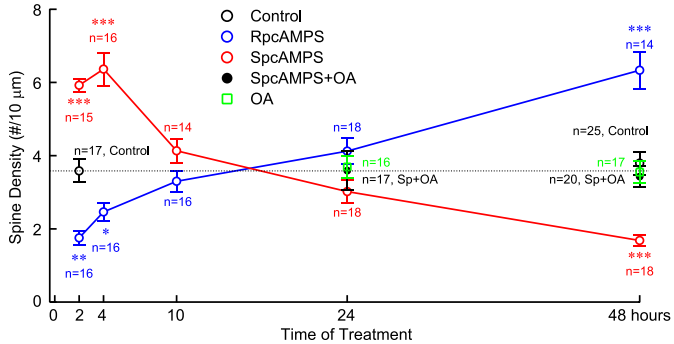

FIGURE 8. **Organotypic hippocampal slice cultures from P6–7 WT pups were transfected after 4–5 DIV with Lck-GFP.** Cultures were treated with 200 μM RpcAMPS, SpcAMPS, and 1 nM okadaic acid (*OA*) for 2–48 h, as indicated. (*n:* number of neurons quantified from 3 independent experiments). RpcAMPS reduces spine density during short term treatments but increases density over 48 h. SpcAMPS increases spine density during short term treatments but decreases density over 48 h. OA has no effect by itself over 24 and 48 h but prevents the decrease in spine density by the 48 h SpcAMPS treatment. *, $p < 0.05$; **, $p < 0.01$; ***, $p < 0.0001$: Bonferroni's multiple comparison with control following ANOVA ($p < 0.0001$).

However, protein levels of other AKAPs are not up-regulated in the KO mice (25). Truncation of the PKA binding site of AKAP150 in D36 mice does not disrupt its overall expression nor its localization to postsynaptic densities (22, 23). It leaves intact the identified binding sites for other binding partners including F-actin, calmodulin, PIP_2, cadherin, adenylyl cyclase, PKC, PSD-95, and PP2B (20, 28, 30, 47–51). As the C-terminally deleted AKAP150 still binds PP2B, the phosphorylation status of postsynaptic proteins might be shifted more toward dephosphorylation in D36 than KO mice upon Ca^{2+} influx, which activates PP2B, with KO but not D36 having lost AKAP150 as a PP2B adaptor (25).

Ectopic expression of AKAP79 fragments indicates that residues 1–361 result in a dominant negative effect but residues 1–153, which bind to F-actin, cadherin, adenylyl cyclase, and PIP_2, and are generally important for subcellular targeting of AKAP79/150, do not (Fig. 7*B*). This dominant negative effect thus requires the central domain (residues 153–315), which interacts with PSD-95 and its homologues (50). It thus appears that the interaction of AKAP79/150 with PSD-95 is important

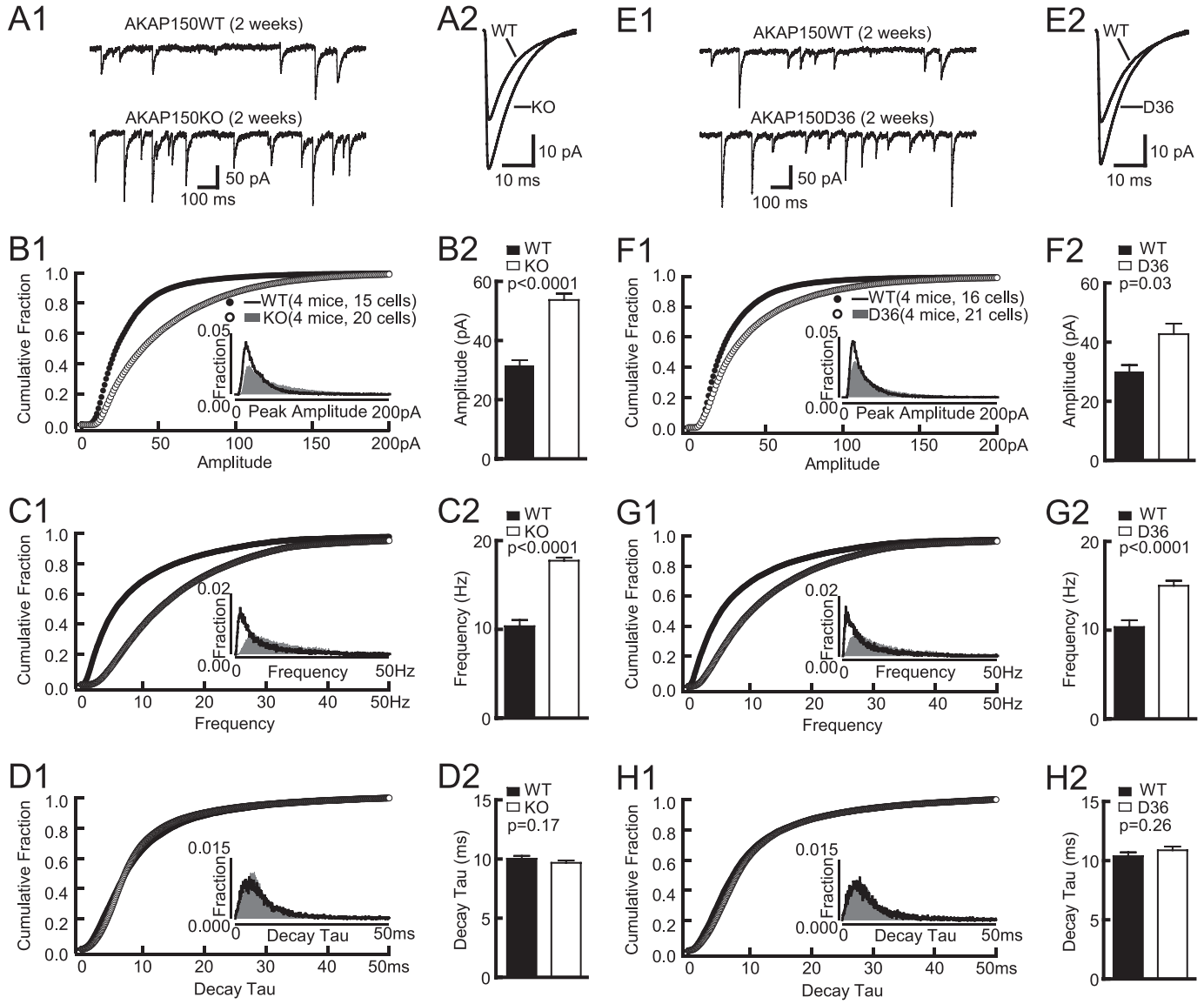

FIGURE 9. *A*, example (*A1*) and averaged (*A2*) mIPSCs from acute hippocampal slices from 2-week-old WT and KO mice. *B*, cumulative fractions (*B1*) and histogram distribution (*inset*) of mIPSC amplitude show a right shift. The amplitude average (*B2*) is significantly increased in KO (53.7 ± 2.2 pA) *versus* WT (31.5 ± 1.8 pA; $p < 0.0001$). *C*, cumulative fractions (*C1*) and histogram distribution (*inset*) of mIPSC frequency show a right shift. The frequency average (*C2*) is significantly increased in KO (17.7 ± 0.3Hz) *versus* WT (10.3 ± 0.7Hz; $p < 0.0001$). *D*, cumulative fractions (*D1*) and histogram distribution (*inset*) of mIPSC decay tau are unaltered in KO. The decay tau average (*D2*) is comparable between KO (9.7 ± 0.2ms) and WT (10.0 ± 0.2ms). *E*, example (*E1*) and averaged (*E2*) mIPSCs from acute hippocampal slices from 2-week-old WT and D36 mice. *F*, cumulative fractions (*F1*) and histogram distribution (*inset*) of mIPSC amplitude show a right shift. The amplitude average (*F2*) is significantly increased in D36 (42.7 ± 3.5 pA) *versus* WT (30.0 ± 2.2 pA; $p < 0.05$). *G*, Cumulative fractions (*G1*) and histogram distribution (*inset*) of mIPSC frequency show a right shift. The frequency average (*G2*) is significantly increased in D36 (15.0 ± 0.6Hz) *versus* WT (10.4 ± 0.8Hz; $p < 0.0001$). *H*, cumulative fractions (*H1*) and histogram distribution (*inset*) of mIPSC decay tau are unaltered in D36. The decay tau average (*H2*) is comparable between D36 (10.9 ± 0.3 ms) and WT (10.4 ± 0.3 ms). *p* values of Mann-Whitney tests are shown in each subpanel.

for the postsynaptic localization of this AKAP. These results are fundamentally different from a spine size- and density-enhancing effect of overexpression of full-length AKAP150 in dissociated hippocampal cultures, which does not depend on PKA anchoring by AKAP150 (50) and likely reflects a fundamental divergence between organotypic slice cultures and dissociated hippocampal cultures. In detail, spine density (but not size) is increased in AKAP150 D36 and KO mice *in vivo* and in organotypic slice cultures (Figs. 2 and 4) but it is decreased upon knock-down of AKAP150 by shRNA in pyramidal cells in primary hippocampal cultures (50). Furthermore, whereas overexpression of full length AKAP79 (residues 1–427) had no effect but overexpression of residues 1–361, which lack the PKA binding site, increased spine density (but not spine size) in organotypic slice cultures (Fig. 7*B*), both constructs increased spine density and size in hippocampal cultures (50). Accordingly, in organotypic slice cultures and *in vivo* the AKAP150 effects reflect loss of PKA anchoring by the C-terminal deletion or KO of AKAP150. In primary hippocampal cultures the effect of overexpression of full-length or C-terminally truncated AKAP150 reflects increased interactions with PSD-95 and its homologues (50), which in turn are known to promote spine size and number. We conclude that in primary cultures overexpression of AKAP150 engages mechanisms different from

those *in vivo* and in organotypic slice cultures, with the spine size and density enhancing mechanisms being prominent mainly in dissociated neuronal cultures but not organotypic slice cultures. It is possible that we did not see an increase in spine density or size upon overexpression of full-length AKAP150 in our slice cultures because the absolute age of neurons in these cultures correspond to P12 at which point in time expression of PSD-95 and its closest homologue, PSD-93, is still very low and starts to increase only a couple of days later *in vivo* and in primary hippocampal cultures (50, 70). It is also conceivable that overexpression of full-length AKAP150 resulted in two opposing effects: a spine promoting activity by acting as a postsynaptic scaffold as described in Ref. 50 and a spine impairing activity by recruiting additional PKA.

Spine density at an adult age is normal in our D36 and KO mice and in a different AKAP150 KO strain (24) (younger ages were not investigated in Ref. 24). The negative effect of PKA on spine density is thus restricted to earlier developmental phases. Homeostatic mechanisms in mature neurons may generate compensatory responses to destabilize the supernumerary spines formed during development. In fact, other studies report that abnormal spine density at young ages is rectified at more mature ages (for recent examples see Refs. 71, 72). Accordingly, spine density is regulated by several powerful mechanisms that ensure normal density at the adult stage if at all possible.

Chronic increases in cAMP cause spine shrinkage via activation of the Rap-GEF EPAC2 in cortical cultures (73). None of the PKA activators or inhibitors we used induced changes in spine size or shape (Fig. 7), but they did induce changes in spine density. The differences could be due to low EPAC2 expression in neurons in early *versus* late postnatal development (74) as the spine alterations described here are restricted to earlier phases of development whereas EPAC2 effects are prominent in older neurons (73). They could also be due to differences in molecular mechanisms that govern spine shape and density in slice *versus* dissociated cultures, as discussed above for the differential effects of AKAP150 overexpression in the two systems.

In summary, we found a novel role of PKA, which acts postsynaptically to limit the density of dendritic spines in the hippocampus *in vivo*. Although the molecular mechanism that underlies this role of PKA has not been identified beyond a critical role of PP2A in the spine-reducing effect of PKA upon its chronic stimulation by SpcAMPS, these findings will point future studies toward identification of postsynaptic PKA targets, potentially actin-interacting proteins, which are important for spine formation and stability.

Acknowledgment—We thank Dr. M. Dell'Acqua (University of Colorado Medical School) for cDNA constructs of AKAP79.

REFERENCES

1. Harris, K. M. (1999) *Curr. Op. Neurobiol.* **9,** 343–348
2. Harris, K. M. (2008) in *Structural and Functional Organization of the Synapse* (Hell, J. W., and Ehlers, M. D., eds) Springer, Heidelberg
3. Nimchinsky, E. A., Sabatini, B. L., and Svoboda, K. (2002) *Annu. Rev. Physiol.* **64,** 313–353
4. Tsay, D., and Yuste, R. (2004) *T. Neurosci.* **27,** 77–83
5. Strack, S., and Hell, J. W. (2008) *Structural and Functional Organization of the Synapse* (Hell, J. W., and Ehlers, M. D., eds) pp. 459–500, Springer, Heidelberg
6. Halpain, S. (2000) *T. Neurosci.* **23,** 141–146
7. Matus, A. (2000) *Science* **290,** 754–758
8. Woolley, C. S., Weiland, N. G., McEwen, B. S., and Schwartzkroin, P. A. (1997) *J. Neurosci.* **17,** 1848–1859
9. Dunaevsky, A., Tashiro, A., Majewska, A., Mason, C., and Yuste, R. (1999) *Proc. Natl. Acad. Sci. U.S.A.* **96,** 13438–13443
10. Lendvai, B., Stern, E. A., Chen, B., and Svoboda, K. (2000) *Nature* **404,** 876–881
11. Matus, A. (2005) *Curr. Opin. Neurobiol.* **15,** 67–72
12. Harvey, C. D., Yasuda, R., Zhong, H., and Svoboda, K. (2008) *Science* **321,** 136–140
13. Tanaka, J., Horiike, Y., Matsuzaki, M., Miyazaki, T., Ellis-Davies, G. C., and Kasai, H. (2008) *Science* **319,** 1683–1687
14. Dailey, M. E., and Smith, S. J. (1996) *J. Neurosci.* **16,** 2983–2994
15. Ziv, N. E., and Smith, S. J. (1996) *Neuron* **17,** 91–102
16. Dunaevsky, A., Blazeski, R., Yuste, R., and Mason, C. (2001) *Nature Neurosci.* **4,** 685–686
17. Engert, F., and Bonhoeffer, T. (1999) *Nature* **399,** 66–70
18. Maletic-Savatic, M., Malinow, R., and Svoboda, K. (1999) *Science* **283,** 1923–1927
19. Toni, N., Buchs, P. A., Nikonenko, I., Bron, C. R., and Muller, D. (1999) *Nature* **402,** 421–425
20. Gomez, L. L., Alam, S., Smith, K. E., Horne, E., and Dell'Acqua, M. L. (2002) *J. Neurosci.* **22,** 7027–7044
21. Smith, K. E., Gibson, E. S., and Dell'Acqua, M. L. (2006) *J. Neurosci.* **26,** 2391–2402
22. Lu, Y., Allen, M., Halt, A. R., Weisenhaus, M., Dallapiazza, R. F., Hall, D. D., Usachev, Y. M., McKnight, G. S., and Hell, J. W. (2007) *EMBO J.* **26,** 4879–4890
23. Lu, Y., Zhang, M., Lim, I. A., Hall, D. D., Allen, M., Medvedeva, Y., McKnight, G. S., Usachev, Y. M., and Hell, J. W. (2008) *J. Physiol.* **586,** 4155–4164
24. Tunquist, B. J., Hoshi, N., Guire, E. S., Zhang, F., Mullendorff, K., Langeberg, L. K., Raber, J., and Scott, J. D. (2008) *Proc. Natl. Acad. Sci. U.S.A.* **105,** 12557–12562
25. Weisenhaus, M., Allen, M. L., Yang, L., Lu, Y., Nichols, C. B., Su, T., Hell, J. W., and McKnight, G. S. (2010) *PLoS One* **5,** e10325
26. Bregman, D. B., Hirsch, A. H., and Rubin, C. S. (1991) *J. Biol. Chem.* **266,** 7207–7213
27. Carr, D. W., Stofko-Hahn, R. E., Fraser, I. D., Cone, R. D., and Scott, J. D. (1992) *J. Biol. Chem.* **267,** 16816–16823
28. Klauck, T. M., Faux, M. C., Labudda, K., Langeberg, L. K., Jaken, S., and Scott, J. D. (1996) *Science* **271,** 1589–1592
29. Coghlan, V. M., Perrino, B. A., Howard, M., Langeberg, L. K., Hicks, J. B., Gallatin, W. M., and Scott, J. D. (1995) *Science* **267,** 108–111
30. Dell'Acqua, M. L., Dodge, K. L., Tavalin, S. J., and Scott, J. D. (2002) *J. Biol. Chem.* **277,** 48796–48802
31. Colledge, M., Dean, R. A., Scott, G. K., Langeberg, L. K., Huganir, R. L., and Scott, J. D. (2000) *Neuron* **27,** 107–119
32. Oliveria, S. F., Gomez, L. L., and Dell'Acqua, M. L. (2003) *J. Cell Biol.* **160,** 101–112
33. Kornau, H. C., Schenker, L. T., Kennedy, M. B., and Seeburg, P. H. (1995) *Science* **269,** 1737–1740
34. Chen, L., Chetkovich, D. M., Petralia, R. S., Sweeney, N. T., Kawasaki, Y., Wenthold, R. J., Bredt, D. S., and Nicoll, R. A. (2000) *Nature* **408,** 936–943
35. El-Husseini, A. E., Schnell, E., Chetkovich, D. M., Nicoll, R. A., and Bredt, D. S. (2000) *Science* **290,** 1364–1368
36. Schnell, E., Sizemore, M., Karimzadegan, S., Chen, L., Bredt, D. S., and Nicoll, R. A. (2002) *Proc. Natl. Acad. Sci. U.S.A.* **99,** 13902–13907
37. Leonard, A. S., Davare, M. A., Horne, M. C., Garner, C. C., and Hell, J. W. (1998) *J. Biol. Chem.* **273,** 19518–19524
38. Tavalin, S. J., Colledge, M., Hell, J. W., Langeberg, L. K., Huganir, R. L., and Scott, J. D. (2002) *J. Neurosci.* **22,** 3044–3051
39. Wong, W., and Scott, J. D. (2004) *Nat. Rev. Mol. Cell Biol.* **5,** 959–970
40. Tavalin, S. J. (2008) *J. Biol. Chem.* **283,** 11445–11452
41. Brooks, I. M., and Tavalin, S. J. (2011) *J. Biol. Chem.* **286,** 6697–6706

42. Banke, T. G., Bowie, D., Lee, H., Huganir, R. L., Schousboe, A., and Traynelis, S. F. (2000) *J. Neurosci.* **20,** 89–102
43. Esteban, J. A., Shi, S. H., Wilson, C., Nuriya, M., Huganir, R. L., and Malinow, R. (2003) *Nature Neurosci.* **6,** 136–143
44. Oh, M. C., Derkach, V. A., Guire, E. S., and Soderling, T. R. (2006) *J. Biol. Chem.* **281,** 752–758
45. Man, H. Y., Sekine-Aizawa, Y., and Huganir, R. L. (2007) *Proc. Natl. Acad. Sci. U.S.A.* **104,** 3579–3584
46. Joiner, M. L., Lisé, M. F., Yuen, E. Y., Kam, A. Y., Zhang, M., Hall, D. D., Malik, Z. A., Qian, H., Chen, Y., Ulrich, J. D., Burette, A. C., Weinberg, R. J., Law, P. Y., El-Husseini, A., Yan, Z., and Hell, J. W. (2010) *EMBO J.* **29,** 482–495
47. Dell'Acqua, M. L., Faux, M. C., Thorburn, J., Thorburn, A., and Scott, J. D. (1998) *EMBO J.* **17,** 2246–2260
48. Gorski, J. A., Gomez, L. L., Scott, J. D., and Dell'Acqua, M. L. (2005) *Mol. Biol. Cell* **16,** 3574–3590
49. Horne, E. A., and Dell'Acqua, M. L. (2007) *J. Neurosci.* **27,** 3523–3534
50. Robertson, H. R., Gibson, E. S., Benke, T. A., and Dell'Acqua, M. L. (2009) *J. Neurosci.* **29,** 7929–7943
51. Efendiev, R., Samelson, B. K., Nguyen, B. T., Phatarpekar, P. V., Baameur, F., Scott, J. D., and Dessauer, C. W. (2010) *J. Biol. Chem.* **285,** 14450–14458
52. Hall, D. D., Davare, M. A., Shi, M., Allen, M. L., Weisenhaus, M., McKnight, G. S., and Hell, J. W. (2007) *Biochemistry* **46,** 1635–1646
53. Gan, W. B., Grutzendler, J., Wong, W. T., Wong, R. O., and Lichtman, J. W. (2000) *Neuron* **27,** 219–225
54. Qin, L., Marrs, G. S., McKim, R., and Dailey, M. E. (2001) *Comp. Neurol.* **440,** 284–298
55. Zha, X. M., Green, S. H., and Dailey, M. E. (2005) *Mol. Cell Neurosci.* **29,** 494–506
56. Marrs, G. S., Green, S. H., and Dailey, M. E. (2001) *Nat. Neurosci.* **4,** 1006–1013
57. Kim, Y., Sung, J. Y., Ceglia, I., Lee, K. W., Ahn, J. H., Halford, J. M., Kim, A. M., Kwak, S. P., Park, J. B., Ho Ryu, S., Schenck, A., Bardoni, B., Scott, J. D., Nairn, A. C., and Greengard, P. (2006) *Nature* **442,** 814–817
58. Han, J., Mark, M. D., Li, X., Xie, M., Waka, S., Rettig, J., and Herlitze, S. (2006) *Neuron* **51,** 575–586
59. Pelkey, K. A., Topolnik, L., Lacaille, J. C., and McBain, C. J. (2006) *Neuron* **52,** 497–510
60. Schulz, P. E., Cook, E. P., and Johnston, D. (1994) *J. Neurosci.* **14,** 5325–5337
61. Zalutsky, R. A., and Nicoll, R. A. (1990) *Science* **248,** 1619–1624
62. Benediktsson, A. M., Schachtele, S. J., Green, S. H., and Dailey, M. E. (2005) *J. Neurosci. Methods* **141,** 41–53
63. Collin, C., Miyaguchi, K., and Segal, M. (1997) *Neurophysiology* **77,** 1614–1623
64. McAvoy, T., Zhou, M. M., Greengard, P., and Nairn, A. C. (2009) *Proc. Natl. Acad. Sci. U.S.A.* **106,** 3531–3536
65. Nicholls, R. E., Alarcon, J. M., Malleret, G., Carroll, R. C., Grody, M., Vronskaya, S., and Kandel, E. R. (2008) *Neuron* **58,** 104–117
66. Nägerl, U. V., Eberhorn, N., Cambridge, S. B., and Bonhoeffer, T. (2004) *Neuron* **44,** 759–767
67. Zhou, Q., Homma, K. J., and Poo, M. M. (2004) *Neuron* **44,** 749–757
68. Ahn, J. H., McAvoy, T., Rakhilin, S. V., Nishi, A., Greengard, P., and Nairn, A. C. (2007) *Proc. Natl. Acad. Sci. U.S.A.* **104,** 2979–2984
69. Turrigiano, G. G., and Nelson, S. B. (2004) *Nat. Rev. Neurosci.* **5,** 97–107
70. Sans, N., Petralia, R. S., Wang, Y. X., Blahos, J., 2nd, Hell, J. W., and Wenthold, R. J. (2000) *J. Neurosci.* **20,** 1260–1271
71. Kim, I. H., Park, S. K., Hong, S. T., Jo, Y. S., Kim, E. J., Park, E. H., Han, S. B., Shin, H. S., Sun, W., Kim, H. T., Soderling, S. H., and Kim, H. (2009) *J. Neurosci.* **29,** 14039–14049
72. Xu, J., Xiao, N., and Xia, J. (2010) *Nature Neurosci.* **13,** 22–24
73. Woolfrey, K. M., Srivastava, D. P., Photowala, H., Yamashita, M., Barbolina, M. V., Cahill, M. E., Xie, Z., Jones, K. A., Quilliam, L. A., Prakriya, M., and Penzes, P. (2009) *Nature Neurosci.* **12,** 1275–1284
74. Ulucan, C., Wang, X., Baljinnyam, E., Bai, Y., Okumura, S., Sato, M., Minamisawa, S., Hirotani, S., and Ishikawa, Y. (2007) *Am. J. Physiol. Heart Circ. Physiol.* **293,** H1662–H1672